

Time-Domain Correlation Quantitative Analysis Method of Regional Rainfall-Landslide Displacement Responses Based on a Time-Domain Correlation Model

Tingchen Wu

Faculty of Geomatics Lanzhou Jiaotong University

Xiao Xie (✉ xiexiao@iae.ac.cn)

Zhejiang Hi-Target Spatial Information Technology Co.,Ltd <https://orcid.org/0000-0002-2598-0047>

Qing Zhu

Faculty of Geosciences and Environmental Engineering Southwest Jiaotong University

YeTing Zhang

Wuhan University State Key Laboratory of Information Engineering in Surveying Mapping and Remote Sensing

Haoyu Wu

Faculty of Geosciences and Environmental Engineering, Southwest Jiaotong University

Haowei Zeng

Faculty of Geosciences and Environmental Engineering, Southwest Jiaotong University

Manuscript

Keywords: Regional Rainfall, Landslide Displacement, Time-domain Correlation Modeling, Quantitative Response Analysis, Impulse Response Function, Signal Correlation

Posted Date: February 4th, 2021

DOI: <https://doi.org/10.21203/rs.3.rs-165789/v1>

License:  This work is licensed under a Creative Commons Attribution 4.0 International License.

[Read Full License](#)

1 ***Ethical Statements**

2 Ethical Statement for Natural Hazards

3 I testify on behalf of all co-authors that our article submitted to Natural Hazards:

4 Title: Time-domain correlation quantitative analysis method of regional rainfall-landslide
5 displacement responses based on a time-domain correlation model

6 All authors: Tingchen Wu; Xiao Xie; Qing Zhu; Yeting Zhang; Haoyu Wu; Haowei Zeng

7 1) This material has not been published in whole or in part elsewhere;

8 2) The manuscript is not currently being considered for publication in another journal;

9 3) All authors have been personally and actively involved in substantive work leading to the
10 manuscript, and will hold themselves jointly and individually responsible for its content.

11 **Authors**

12 Tingchen Wu [First Author]

13 Faculty of Geomatics, Lanzhou Jiaotong University, Lanzhou 730070, China

14 Faculty of Geosciences and Environmental Engineering, Southwest Jiaotong University, Chengdu
15 611756, China

16 Email: giswtchen@163.com

17 ORCID: 0000-0002-0777-3247

18 Xiao Xie [Corresponding Author]

19 R&D Department , Zhejiang Hi-Target Spatial Information Technology Co., Ltd., Huzhou 313200, China

20 Sichuan Visual Smart Map Spatial Information Technology Co., Ltd., Chengdu 610036, China

21 Email: xiexiao@iae.ac.cn

22 ORCID: 0000-0002-2598-0047

23 Qing Zhu

24 Faculty of Geosciences and Environmental Engineering, Southwest Jiaotong University, Chengdu
25 611756, China

26 Sichuan Visual Smart Map Spatial Information Technology Co., Ltd., Chengdu 610036, China

27 Email: zhuq66@263.net

28 Yeting Zhang

29 Wuhan University State Key Laboratory of Information Engineering in Surveying, Mapping and
30 Remote Sensing, Wuhan 430079, China;

31 Email: zhangyeting@whu.edu.cn

32 Haoyu Wu

33 Faculty of Geosciences and Environmental Engineering, Southwest Jiaotong University, Chengdu
34 611756, China

35 Email: haoyu.wu@my.swjtu.edu.cn

36 Haowei Zeng

37 Faculty of Geosciences and Environmental Engineering, Southwest Jiaotong University, Chengdu
38 611756, China

39 Email: zenghaowei@my.swjtu.edu.cn

40 Time-domain correlation quantitative analysis method of regional
41 rainfall-landslide displacement responses based on a time-domain
42 correlation model

43 **Abstract** Landslide deformation is the most intuitive and effective characterization of the evolution of
44 landslides and reveals their inherent risk. Considering the inadequacy of existing deformation monitoring
45 data in the early warning of landslide hazards, resulting in insufficient disaster response times, this paper
46 proposes a time-domain correlation model. Based on a regional rainfall-landslide deformation response
47 analysis method, a time-domain correlation measure between regional rainfall and landslide deformation
48 and a calculation method based on impulse response functions are proposed for prevalent rainfall-
49 induced landslide areas, and the correlation with the rainfall-triggered landslide deformation mechanism
50 is quantitatively modeled. Furthermore, using rainfall monitoring data to optimize the indicator system
51 for landslide deformation monitoring and early warning significantly improves the preliminary warning
52 based on landslide deformation. The feasibility of the method proposed in this paper is verified by
53 analyzing the historical monitoring data of rainfall and landslide deformation at 15 typical locations in 5
54 landslide hidden hazard areas in Fengjie County, Chongqing city. (1) The correlation models for the XP
55 landslide and XSP landslide involve a 5-day lagged correlation under a 56-day cycle and a 18-21-day
56 lagged correlation under a 49-52-day cycle, which means that the deformation in the above areas can be
57 modeled cyclically according to monitoring data, and early landslide warnings can be provided in
58 advance with a lag time. (2) The correlation models for the TMS landslide and OT landslide show
59 consistent correlations under a 48-50-day cycle and a 58-day cycle, which means that the deformation in
60 the above areas can be predicted based on rainfall accumulation, and real-time warnings of future
61 landslide deformation and displacement can be obtained. (3) The HJWC landslide presents a disorderly
62 correlation pattern, which means that a preliminary landslide deformation warning cannot be provided
63 based on rainfall alone; other monitoring data need to be supplemented and analyzed.

64 **Keywords:** Regional Rainfall; Landslide Displacement; Time-domain Correlation Modeling;
65 Quantitative Response Analysis; Impulse Response Function; Signal Correlation

66 **Foundation:** The National Key Research and Development Program of China (No. 2018YFB0505404)

67 **Introduction**

68 Regional rainfall-triggered landslides, which are characterized by large masses, instantaneous
69 sliding, and violent and large extents of damage, are one of the main types of geological disasters in
70 China(Yuan 2005, Yue-li et al. 2016, Ze-lin et al. 2020). Statistically, most of the main landslides that
71 have occurred in Southwest China over the past 40 years were caused by rainfall, which is the main cause
72 of the instability of such landslides(Qiu-xiang et al. 2020). Hence, landslide deformation monitoring data
73 provide important information for the early warning of various landslide risks and for uncovering the
74 key moments of landslide events for their prevention and control(ZHU Qing 2017, Yan et al. 2019, Du
75 et al. 2020). However, because landslides characteristically accumulate deformation slowly and occur
76 instantaneously, it is difficult to achieve a forward-looking landslide risk warning system through only
77 deformation monitoring data; accordingly, the development of additional early warning methods is urgent.

78 The existing landslide early warning analysis models mainly include dynamic analysis models and
79 logistic regression models. Dynamic analysis models are calculation schemes based on the physical
80 mechanisms of events(Li and Zhao 2019, Zhiyun et al. 2020); hence, these models are limited to data
81 from the test site or to the research and exploration of a single landslide area and thus cannot meet the
82 requirements for investigating landslide groups in different geological environments(Shu-lin et al. 2020,
83 Tao et al. 2020). In contrast, logistic regression models employ mathematical statistics to perform logistic
84 regression and determine the critical value of landslide rainfall and the probability of landslide
85 occurrence(Yi-ting et al. 2015, ADINEH et al. 2018); however, this method is suitable only for small-
86 scale quantitative research and cannot be used for different categories.

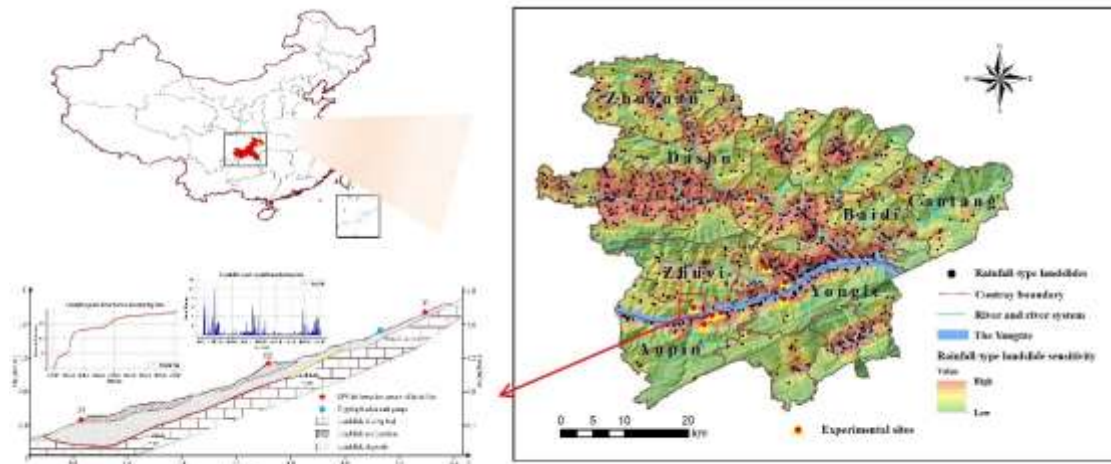
87 Rainfall-triggered landslides have been summarized and classified; as a result, the data accuracy
88 requirements are too high, and the calculations are too complicated to meet the warning requirements. In
89 view of these limitations, the combined use of geomechanics, physical mechanics, and numerical analysis
90 models to evaluate the stability of landslides during rainfall events can help predict the development
91 trend of landslides, but the corresponding workload is often large, leading to delays in warnings. As an
92 alternative approach, the monitoring data of landslide deformation characteristics and the rainfall factor,
93 which is the main influence on the landslide process, often have obvious correlations(Ferro et al. 2020,
94 Yin et al. 2016, De-ying et al. 2019). Therefore, it is feasible to predict the risk of landslides by using
95 widely available rainfall monitoring data. Accordingly, establishing an effective correlation model
96 between regional rainfall and landslide deformation monitoring data and thereby achieving quantitative
97 correlations have become key issues for effectively improving the timeliness of landslide early warnings.

98 In response to the above problems, this paper proposes a time-domain method for the quantitative
99 analysis of the regional rainfall-landslide deformation response. First, according to the seasonal and
100 hysteresis variations of landslide deformation during the infiltration of rainfall into the ground, Using
101 easily accessible regional rainfall and landslide deformation monitoring data, this paper proposes the
102 concept of correlation measures between the two in the time domain to measure the correlation period
103 and signal time shift(Adel et al.); on this basis, the correlation is computed by using the impulse response
104 functions of different characteristics in the signal processing algorithm; Finally, the landslide deformation
105 response to rainfall is quantitatively analyzed. The time-domain correlation model includes a consistency
106 model, a hysteresis model and a disorder model. The proposed method can be applied to historical
107 monitoring data from different areas characterized by hidden landslide hazards; then, the corresponding
108 correlation models can be analyzed and summarized, and the time-domain correlation between the
109 regional rainfall and the deformation of a hidden landslide hazard point can be quantitatively calculated
110 as a reference to predict the future deformation of the landslide affected by rainfall. This method provides
111 a scientific basis for pre-warning systems by effectively extending the time allowed in the early warning
112 of landslides.

113 **Study area**

114 The experimental area adopted in this paper is within Fengjie County in eastern Chongqing (between
115 109°1'17" and 109°45'58" east longitude and 30°29'19" and 31°22'23" north latitude). Fengjie County,
116 located on the eastern edge of the Sichuan Basin (Figure 1), represents the central hinterland of the Three
117 Gorges Reservoir. The study area is in the city of Chongqing and the Yangtze River Three Gorges Project,
118 and the rainfall and environment are closely related(Yin et al. 2016, Tiping et al. 2014). ①The river
119 flowing through Fengjie County is the Yangtze River, and the county has abundant rainfall with a heavy
120 rainstorm intensity and is characterized by large accumulations of rainfall in a short time and a high
121 erosion intensity. In addition, the distributions of landslides and cumulative rainfall (or strong triggering
122 rainfall) are consistent. The minimum cumulative rainfall for landslides is 200 mm. ②The geological
123 environment in the study area is relatively fragile. The terrain provides good conditions for surface water
124 infiltration, surface water migration, and the occurrence of landslides③The regional landforms are
125 mainly moderately eroded mountain and middle-low mountain landforms and eroded hilly landforms
126 with high hills, large undulations, and steep slopes; developed landslides are also prominent. The
127 sensitive slope is 20°~30°, and landslides tend to occur at elevations of 400~1000 m. This paper selects
128 five rainfall-triggered landslides, including the OT landslide, XP landslide, and HJWC landslide, and a
129 total of 15 representative monitoring points for experiments. Table 1 lists the various monitoring points,
130 which will verify that the method proposed in this paper is suitable with adaptable applicability for

131 different landslide scenarios under diverse conditions.



132
133 **Fig.1** The tests were conducted at rainfall-triggered landslides such as the Xinpu landslide in Fengjie County, Chongqing,
134 China
135

136 **Table 1** A qualitative description of the landslide area and monitoring points in the test (partly collected from the literature). Will be used for the quantitative analysis in this paper

Landslide area	Type of landslide	Monitoring sites	Location of Monitoring sites	Landslide environment (① rock formations ② hydrogeology ③ human)
TMS landslide(Gang)	Shallow wading landslides	1220	Leading edge of slide blocking section	① Mainly composed of gravelly clay and gravelly soil rocks; ② Poor groundwater storage conditions, direct infiltration to recharge the bedrock fracture water; ③ Shear outlet near the water system, no surrounding houses, roads, etc.
		1235	Index segment antecedents	
		1243	Leading and trailing edges of lower sliding section	
OT landslide(Huan 2016)	Giant cis-laminated rocky paleo landslide	MJ01	Leading edge of slide blocking section	① Mainly composed of powder clay sandwiched between crushed boulders, etc., the physical and mechanical properties of the stratum are highly variable; ② The material permeability of the landslide body is good, and a large amount of precipitation permeates through the surface to increase the self-weight and sliding force of the landslide body; ③ Located in Anping Town on the right bank of the Yangtze River, near the Three
		MJ14	Leading edge of slide blocking section	
		FA35	Landslide shear outlet	

		Gorges Reservoir.		
XP landslide(Shen 2011)	Grade I Very Large Earth Slide	GDA10068	Leading edge of slide blocking section	①Moderately weathered - strongly weathered marl and tuff dominate;
		GDA10077	Index segment antecedents	② The front edge is continuously washed by the water of the Yangtze River and the mechanical properties of the whole slope are reduced; ③
		GDA10057	Leading and trailing edges of lower sliding section	The landslide is located on the left bank of the Yangtze River, near the densely populated market town of Anping Township.
XSP landslide(Xin 2016)	Thick layer traction-push downhill slides	FJ02	Leading edge of slide blocking section	①The slope is mainly composed of sandstone chalky clay and gravelly soil rocks; ②The sudden cracking of the back edge of the slope soil caused by rainfall induced landslides; ③ There are a few houses and roads around.
		FJ03	Index segment antecedents	
		FJ04	Landslide shear outlet	
HJWC landslide(Yang et al. 2012)	Medium cascading bedrock landslide	FJ02	Leading edge of slide blocking section	①Mainly composed of laminated mudstone, muddy siltstone and sandy tuff; ②Groundwater within the landslide area is mainly overburden pore water, influenced by atmospheric precipitation, with large seasonal variations; ③Near the Three Gorges Reservoir, the main part of the new site of Shuanglong Town is located on this landslide body.
		FJ05	Index segment antecedents	
		FJ09	Leading and trailing edges of lower sliding section	

137

138 Data and methods

139 Data

140 The experimental data in this paper consist of landslide surface deformation data and regional
 141 rainfall data obtained from 2017 to 2020 at the Fengjie regional monitoring point, provided by Chongqing
 142 Planning and natural resources Bureau. The deformation variable is the vertical surface displacement
 143 monitored by geodetic GPS instruments. The time interval is an hour, and the rainfall is recorded in an
 144 hourly increment by a tipping bucket, and the data are unified in time sequences with a unit of days
 145 during data preprocessing.

146 Methods

147 The properties of the soil and rock comprising the landslide body in different regional environments

180 deformation. With the correlation time measurement T , the conditions under which a landslide occurs
 181 can be quantitatively expressed as the following formula:

$$182 \quad T = t_s(D_s - R_a) \quad (1)$$

183 (2) Signal time shift (td). Because landslides occur in areas with heterogenous geological conditions, the
 184 deformation lags behind the precipitation due to the infiltration of rainfall (Vallet et al. 2016). According
 185 to research on the complicated mechanism responsible for level water flow within a landslide body, the
 186 nature of this delay behind the rainfall is essentially determined by the time when the water enters the
 187 sliding body. The time shift td in Figure 1 is used as a time-domain measure to quantitatively summarize
 188 the response (namely, the correlation period T) of landslide deformation to rainfall events and is
 189 quantitatively expressed as the following formula:

$$190 \quad td = t_s(D_s - R_a) \quad (2)$$

191 The product between the correlation period T and the sampling duration t_s , that is, the time shift td of
 192 the lagged signal, can be correlated with the estimated future deformation of the landslide with the real-
 193 time rainfall ahead of a lag time.

194 The abovementioned critical value R_a of rainfall-triggered deformation is extracted by quantitatively
 195 partitioning the regional rainfall history curve to extract the time-domain characteristics of the triggering
 196 event at different stages. Formula (3) represents the rainfall interval curve partitioned by determining the
 197 average rainfall of each rainfall event. Then, considering the objective environmental factors such as the
 198 regional rock composition, surface shape, and soil quality, the effective rainfall coefficient k (Chen et al.
 199 2016) is established to calculate R_a as the key parameter of the correlation period T , as shown by T in
 200 Figure 2.

$$201 \quad \begin{cases} \bar{R} = \frac{\sum_{i=1}^n R_i}{R_{t_i}} \\ R_a = k\bar{R} \end{cases} \quad (3)$$

202 The above formula for \bar{R} signifies the average rainfall in days calculated by counting the n rainfall
 203 events in the area and the number of rainfall days R_{t_i} . The effective rainfall coefficient k represents the
 204 rainfall retention capacity of the rock and soil and is determined by the regional properties of the rock
 205 and soil.

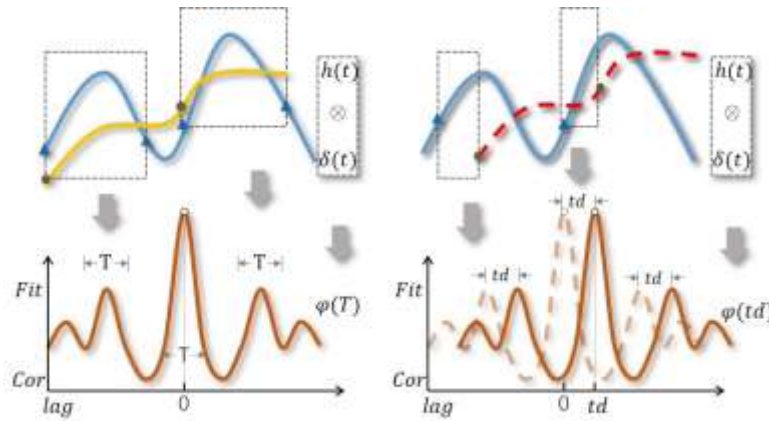
206 Considering the mutation point D_s of landslide deformation, a large number of landslide examples
 207 confirm that landslides, especially gravity-driven landslides, can basically meet the three-stage
 208 deformation law proposed by Saito (Saito 1989), namely, initial deformation, followed by constant-
 209 velocity deformation and ultimately accelerated deformation. On this basis, the variation in the curve
 210 through the deformation analysis is shown in Figure 2. The long time sequence of the landslide
 211 deformation response process can be discerned on the basis of whether the signal curve is initially steady
 212 before experiencing a sudden increase, reaches its peak, and then becomes stable again. Combined with
 213 this principle of signal mutation, the abnormal deformation response point D_s is calculated as the key
 214 parameter of the signal time shift td , and the corresponding formula is expressed as follows:

215 When the signal mutation rate mr is the maximum signal curvature of the overall performance of the
 216 landslide in this area, the landslide surface produces abnormal deformation. When the sudden rise in
 217 deformation has ceased, a moment will come when the phased maximum of accumulated deformation

218 will be generated, after which the landslide evolution process will enter a stable surface deformation
 219 stage.

$$220 \quad \begin{cases} mr = \frac{D_j - D_{j-1}}{D_{-t_j} - D_{-t_{j-1}}} \\ D_{-s} = mr_{-t} \left(\frac{mr}{mr_{-1}} \xrightarrow{\max} \frac{mr_r}{mr_{r-1}} \right) \end{cases} \quad (4)$$

221 To obtain a credible time-domain correlation measure, it is necessary to extract the signal waveform
 222 characteristics of the landslide deformation response process, further calculate the constituent parameters
 223 of the correlation measure to obtain the value interval, and introduce the impulse response function
 224 during the signal processing phase to calculate the specific measured value, as depicted in Figure 3.



225
 226

Fig.3 Schematic diagram for calculating time-domain correlation measures based on impulse response functions

227 However, it is quite difficult to calculate the abovementioned rainfall critical value and landslide
 228 mutation point by partitioning the rainfall history curve into multiple processes. At the same time, the
 229 monitoring data of a complex sequence cannot be satisfied due to signal noise, a delay in the response
 230 and other problems. To accurately fit the correlation measurement of landslides affected by a long-time
 231 sequence of rainfall in reality, the impulse response function is introduced during signal processing to
 232 calculate the correlation function between the two signal sequences and measure the similarity between
 233 the two signals, thereby realizing inversion from geometric distance to the actual time interval (Mucchi
 234 et al. 2004, Mbachu 2020). The impulse response function is a cross-correlation function that describes
 235 the characteristics of the time-domain system and is widely used in radar, sonar, digital communication
 236 and geology (Van 2014). The advantage of the impulse response function is that the algorithm parameters
 237 and convolution operation are suitable for signals mixed with additive noise or delayed samples. For a
 238 given time sequence, this function can solve for the distance of a real target submerged in noise. In the
 239 landslide deformation signal time system continuously affected by regional rainfall, the time series
 240 rainfall monitoring signal R_t without random noise is represented by the continuous impulse signal
 241 $h(t)$. Similarly, when the input signal is the impulse signal $\delta(t)$ of the landslide deformation fitted
 242 waveform, the output response function $\varphi(t)$ of the system is the convolution integral between the input
 243 rainfall sequence and the deformation sequence. According to the specific change in the signal under the
 244 correlation measurement, the response function is divided into a periodic impulse function and a delay
 245 response function.

246 (1) Impulse period function $\varphi(T)$. In the definition of the relevant time parameters of the response
 247 function, the signals $h(t)$ and $\delta(t)$ are assumed to start at the same time due to the obvious existence
 248 of persistent precipitation. When the input rainfall signal shows a periodically repeating waveform, the

249 nonlinear subsystem impulse response function is calculated by the periodic input signal with different
 250 amplitudes as the response function for measuring the rainfall-landslide deformation correlation period.
 251 (2) Delay response function $\varphi(td)$. When the rainfall impulse signal pair and the deformation pulse
 252 signal have a relative offset (lag) on the time axis, their related time parameters will also change. This
 253 dependence is described by a shift function based on the signal with zero padding while considering the
 254 pulse period, as shown in the following formula:

$$255 \left\{ \begin{array}{l} \varphi(T) = \int_{-\infty}^{\infty} \delta(T)h(T - \Delta T)d(\Delta T) \\ \varphi(td) = \int_{-\infty}^{\infty} \delta(T)h(T - td - \Delta T)d(\Delta(td + T)) \end{array} \right. \quad (5)$$

256 Integrating the abovementioned regional rainfall with the landslide deformation correlation
 257 measurement analysis and calculation method, the deformation mechanism and correlation properties of
 258 rainfall-triggered landslides can be broadly classified based on the regional monitoring data, as shown in
 259 Table 2.

260 (1) Rainfall-landslide deformation consistency model (M_1): Under the action of rainfall and infiltration,
 261 the regional surface balance is easily damaged, and sliding occurs. The effect is expressed as a slow and
 262 long-term surface deformation process, as a rainfall process, and as a deformation process. There is good
 263 temporal consistency between the correlation period T and the pulse period function $\varphi(T)$, and the cross-
 264 correlation and the goodness of fit under the correlation period are the largest. This type of model can
 265 determine the real-time landslide deformation and future displacement based on the predicted
 266 accumulation of rainfall.

267 (2) Rainfall-landslide deformation hysteresis model (M_2): Affected by factors such as the composition
 268 of the geological body, the thickness of the landslide body, etc., rainfall-triggered landslide deformation
 269 occurs mostly during the middle and late periods of rainfall or several days later, and the lag times of
 270 different types of landslides differ; that is, there is a lag time td and a delay response function $\varphi(td)$.
 271 Generally, the lag times of landslides that occur in accumulated soil, landfills, loess, clay, clastics and
 272 bedrock range from short to long, and the thickness of the same type of landslide ranges from thin to
 273 thickness.

274 (3) Rainfall-landslide deformation turbulence model (M_3): Because landslide deformation is a slope
 275 displacement caused by the coupling of multiple factors, some landslide areas may exhibit little rainfall
 276 or weak deformation responses to rainfall; that is, there is a discrepancy in the correlation between the
 277 landslide response and rainfall. Such situations cannot be accurately forecasted, and early warning
 278 systems based on rainfall will fail to predict these landslides.
 279

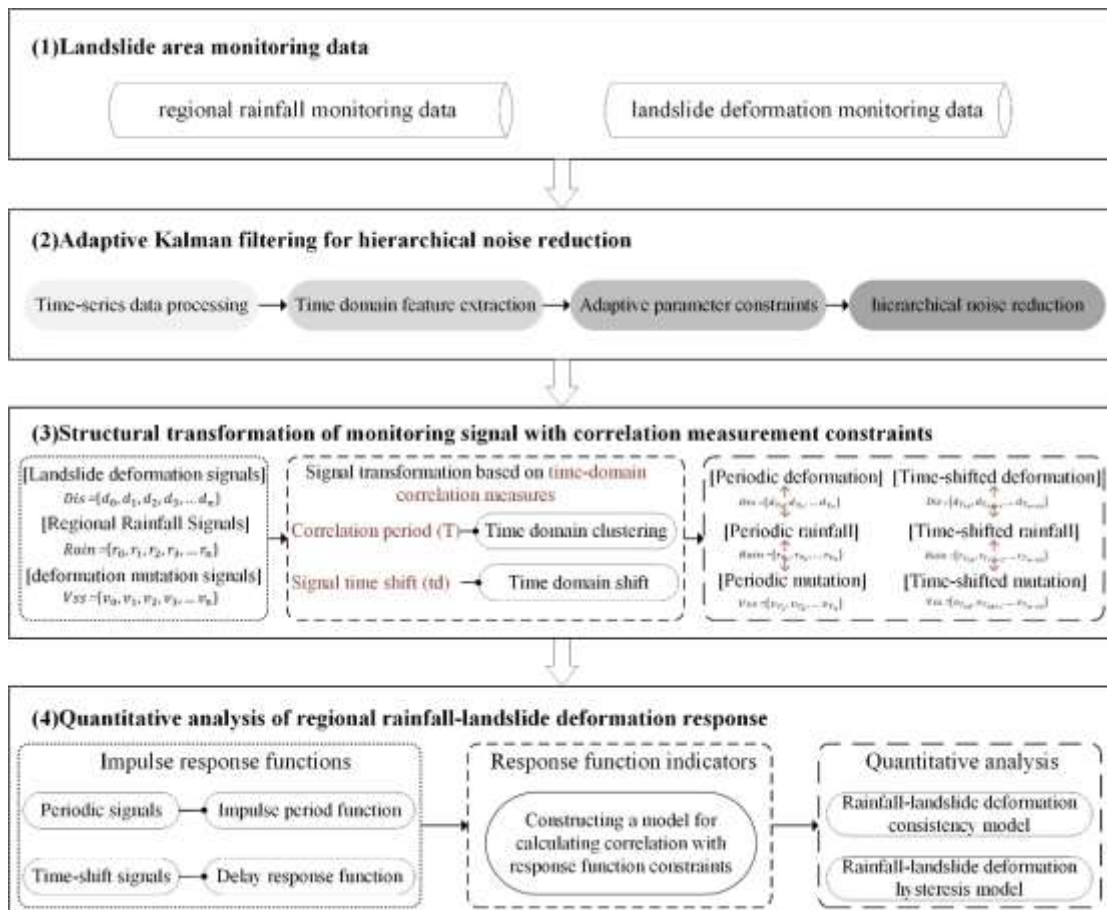
Table 2 Time-domain correlation model of regional rainfall and landslide deformation

	t	$\varphi(t)$	$Cor_{(t T, td)}$	$Fit_{(t T, td)}$
M_1	T	$\varphi(T)$	$Cor_T > Cor_{td}$	$Fit_T > Fit_{td}$
M_2	t	$\varphi(td)$	$Cor_{td} > Cor_T$	$Fit_{td} > Fit_T$
M_3	t	/	$Cor_t < 0.6$	$Fit_t < 0.6$

280 Analysis algorithm of the regional rainfall-landslide deformation response based on the time-domain
 281 correlation model

282 This paper uses signal processing technology to quantitatively measure the correlation between
 283 regional rainfall and landslide deformation. The flow chart of the method is illustrated in the figure below.

284 The core steps are as follows: ①Considering the presence of noise in landslide deformation monitoring
 285 data, the proposed method is based on the described time-domain correlation measurement and parameter
 286 extraction of the change characteristics of rainfall data and deformation data; this approach adopts an
 287 adaptive variable-parameter constrained time-domain classification method for Kalman filtering. ②Due
 288 to the unsynchronized time-domain correlation characteristics between rainfall and deformation in
 289 landslide disasters, combined with the abovementioned correlation measure, the correlation between the
 290 period and time shift of the monitoring signal transformation structure is realized after noise reduction.
 291 ③An impulse response function that can fuse two or more signal time-domain change characteristics is
 292 constructed, and the deformation time series variable is calculated in response to the consistent
 293 correlation and goodness of fit of the rainfall variables. ④The correlation model of the rainfall-landslide
 294 deformation response in combination with the above quantitative factors is analyzed, and then the nature
 295 of the internal factors is verified; finally, the correlation period between regional rainfall and landslide
 296 deformation (the lag time) is quantitatively measured.



297
 298 **Fig.4** Flow chart of the regional rainfall-landslide deformation quantitative response analysis algorithm

299 For landslide disasters in different regions, when using monitoring data to analyze, process and
 300 predict landslide disasters, there is often a certain error between the observed value and the actual value.
 301 How to effectively eliminate this error while retaining the local characteristics is very important in

302 analyzing the deformation characteristics of the landslide. In this paper, the Kalman filtering method is
 303 used to predict the subsequent time-domain state characteristics through the preliminary time-domain
 304 state characteristics and then to combine the observed values to solve for the optimal value, thereby
 305 reducing noise while retaining local feature values.

306 First, the regional rainfall data and landslide deformation monitoring data are processed in a unified time
 307 series; that is, the time series quantity t_{norm} , rainfall r_{norm} , and deformation variable d_{norm} (unit: days)
 308 are obtained. For the geological environment, the rainfall coefficient k is computed, and then the interval
 309 threshold and the mutation signal v_{norm} are calculated according to the rainfall critical value R_a and
 310 the mutation point D_s described in formula (3). Finally, the interval is used to perform adaptive Kalman
 311 filtering for hierarchical noise reduction on the mutation signal according to the following formula(Wang
 312 et al. 2016):

$$313 \quad \begin{cases} F_t = \begin{bmatrix} 1 & \Delta t \\ 0 & 1 \end{bmatrix} \xrightarrow{R_a} \begin{bmatrix} 1 & t_{norm} - t_{norm-1} / R_a \\ 0 & 1 \end{bmatrix} \\ B_t = \begin{bmatrix} \frac{\Delta t^2}{2} \\ \Delta t \end{bmatrix} \xrightarrow{R_a} \begin{bmatrix} \frac{[t_{norm} - t_{norm-1} / R_a]^2}{2} \\ t_{norm} - t_{norm-1} / R_a \end{bmatrix} \\ \hat{v}_{norm} = F_t \times v_{norm} + B_t \times \hat{v}_{norm-1} \end{cases} \quad (6)$$

314 In the above formula, F_t and B_t are the state change matrices in the Kalman filter, Δt is the sampling
 315 time, \hat{v}_{norm} is the current estimate, v_{norm} is the measured value, and \hat{v}_{norm-1} is the previous estimate.

316 Because of the seasonal cyclic characteristics of regional rainfall and the asynchronous time-domain
 317 correlation between rainfall and deformation in landslide hazards, the combined time-domain waveforms
 318 cannot be judged directly, and this paper uses the time-domain correlation measure as a dynamic
 319 parameter to transform the monitoring signals into a characteristic structure for the quantitative analysis
 320 of regional rainfall-landslide deformation response. Eq. (7) clusters the noise-reduced deformation
 321 signals, sudden change signals and rainfall signals based on the correlation period T (Ski and Owczarek
 322 2005). The monitoring signals are divided into several effective time regions by expanding the time series
 323 quantity t_{norm} , while the following signal shifts are further applied to the rainfall signals that have been
 324 clustered in the time domain according to the time shift quantity td , with the aim of further investigating
 325 whether there is a lag between the rainfall and deformation in the region whether there is a lag between
 326 rainfall and deformation in the region.

$$327 \quad \begin{cases} f_T : t_i^T = t_0^{norm} + i \times T \\ d_i^T = f_T [\hat{d}^{norm}] \\ r_i^T = f_T [r^{norm}] \\ \hat{v}_i^T = f_T [\hat{v}^{norm}] \end{cases} \Rightarrow \begin{cases} g_{T-td} : t_i^{T-td} = f_T [t^{norm} - td] \\ d_i^{T-td} = g_{T-td} [\hat{d}^{norm}] \\ r_i^{T-td} = g_{T-td} [r^{norm}] \\ \hat{v}_i^{T-td} = g_{T-td} [\hat{v}^{norm}] \end{cases} \quad (7)$$

328 To calculate the time-domain correlation measure of regional rainfall-landslide deformation, the
 329 following formula combines the signals with the transformed structure to construct a periodic impulse
 330 function and a time-delayed impulse function. Based on the correlation model of the response function,
 331 formula (8) calculates the correlation Cor and degree of fit (labeled Degree Fit)(Dong et al. 2012), which
 332 are used to quantitatively analyze the complex correlation model between landslide deformation and

333 rainfall. According to the model judgment table, a consistent correlation model judgment does not need
 334 to consider the time-domain shift. The signal is expanded and contracted on the basis of the overall
 335 correspondence, the response function index between the two curves is solved with the expanded data,
 336 and the correspondence is adjusted simultaneously to reconstruct the signal. As shown in the formula (9),
 337 multiple sets of correlations are solved in this manner, and the best set is taken for further analysis. In
 338 contrast, the determination of the lag correlation is different from that of the consistent correlation in that
 339 the time-domain shift needs to be considered. When the signal is expanded and contracted, the time-
 340 domain shift is applied to solve for the correlation, and the degree of fit is compared corresponding to
 341 the time-domain response correlation model. The quantitative values of the correlation period T and
 342 signal time shift t_d are then calculated backward.

$$343 \quad \begin{cases} Cor_{\langle t|T,td \rangle} = \sum_{i=0}^{N-1} \delta_i(t) h_{i+t}(t) \\ Fit_{\langle t|T,td \rangle} = \frac{\sum_{j=0}^N (\varphi_i(t) - \delta_i(t))^2}{\sum_{j=0}^N (\varphi_i(t) - h_i(t))^2} \end{cases} \quad (8)$$

$$344 \quad \begin{cases} \varphi(T) = \int_{-\infty}^{\infty} v_i^T r_i^T d(\Delta T) \Rightarrow \begin{cases} Cor_T = Cor(v_i^T, r_i^T) \\ Fit_T = Fit(\varphi(T), v_i^T) \end{cases} \\ \varphi(td) = \int_{-\infty}^{\infty} v_i^T r_i^T d(\Delta(td + T)) \Rightarrow \begin{cases} Cor_{td} = Cor(v_i^T, r_i^{T-td}) \\ Fit_{td} = Fit(\varphi(td), v_i^T) \end{cases} \end{cases} \quad (9)$$

345 Results

346 This paper selects all the GDA10068 monitoring points in the XP landslide area for a quantitative
 347 analysis using the proposed time-domain correlation model, as shown in Figure 5, and simultaneously
 348 calculates the analysis results at all the monitoring points in the landslide area. First, for the original
 349 monitoring data of rainfall and landslide deformation with an hourly sampling interval, the cumulative
 350 amount of which is less than one day due to missing data, interpolation is applied to standardize the units
 351 to days to obtain continuous deformation cumulative signals and rainfall signals. The parameters D_s
 352 and R_a of the time-domain correlation measurement described according to formula 3 and formula 4,
 353 respectively, are then calculated, and the rainfall coefficient k is obtained based on previous research
 354 experience in conjunction with the geological environment of the landslide area (Table 1), and the results
 355 are shown in Table 3. The gain parameter of the Kalman filter is further updated according to formula (6)
 356 to realize adaptive hierarchical noise reduction for the landslide deformation signal. The experimental
 357 effect of this filter is shown in Figure 5.

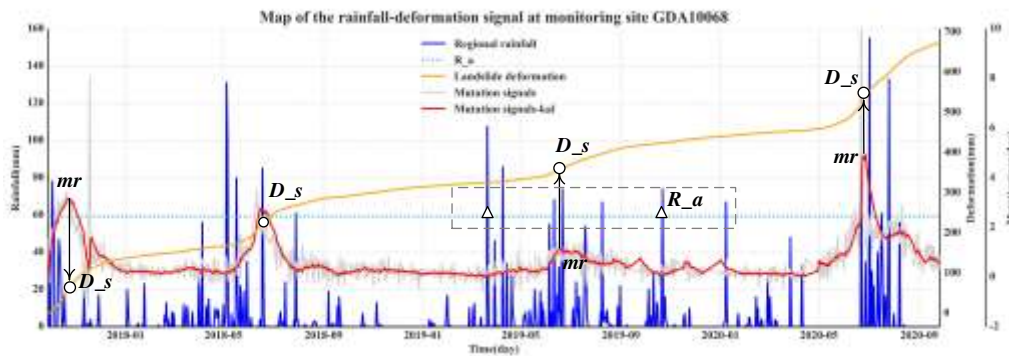
358 **Table. 3** Time domain measurement parameters of monitoring points in landslide area

Monitoring sites	D_s	\bar{R}	k	R_a
1220	1.7628			
1235	1.3285	18.283	6.67	121.94
1243	0.9477			
MJ01	2.6552			
MJ14	2.9282	15.391	9.74	149.90
FA35	2.1681			
GDA10068	2.1371			

GDA10077	2.3757	15.398	12.48	192.16
GDA10357	1.5635			
FJ02	2.3611			
FJ03	2.7911	13.764	11.89	163.65
FJ04	1.3659			
FJ02	10.2612			
FJ05	9.3689	4.404	7.76	34.17
FJ09	10.2251			

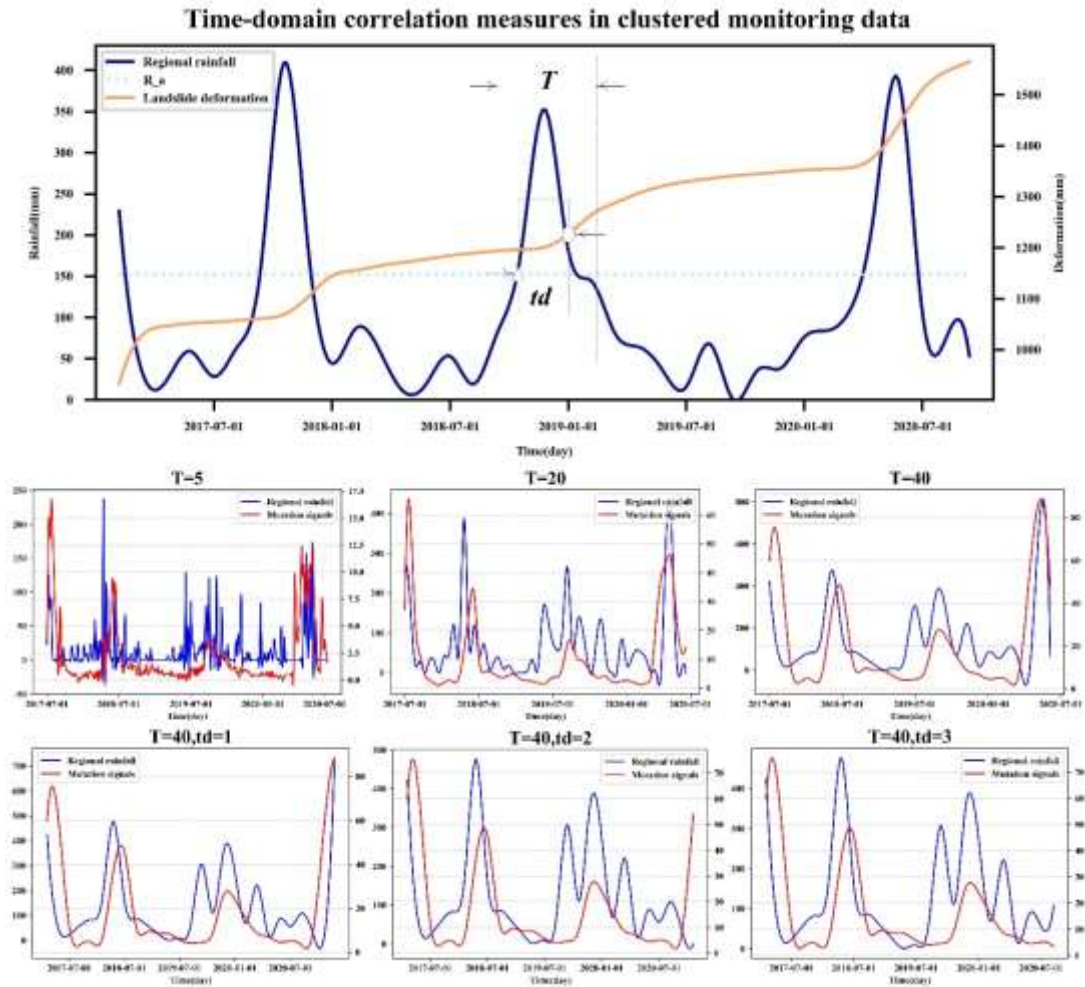
359 In the signal feature structure transformation stage, the time-domain correlation measures T and td
360 are used as variable parameters in formula (7), and the ranges are specified here as 0~60 days and 0~30
361 days, respectively. The example diagram in Figure 5(a) is the feature map of signal clusters at 5, 20, and
362 40 days. At the same time, a certain clustering parameter is fixed, and td is 1, 2 and 3 for the signal time
363 shift. It is obvious that most of the monitoring points in each area record the amount of rainfall, and the
364 deformation signals gradually show the same trend. The correlation degree Cor in formula (8) is used to
365 accurately quantify the accurate value or effective range of the time-domain correlation measure , and
366 the results are shown in Figure 6(b).

367 In the quantitative analysis of the regional rainfall-landslide deformation response, the correlation
368 function between the rainfall and deformation is constructed according to formula (5) using the rainfall-
369 deformation correlation signal after a series of processing steps. The function performance is shown in
370 example Figure 6(c), and the described impulse response function type corresponds and divides the
371 correlation function of the research point into a pulse period function, a delay response function and a
372 disorder function without changing the properties. Using formula (9), the degree of fit can then be
373 calculated to determine the accurate value or effective range of the time-domain correlation measure.
374 Corresponding to the proposed time-domain correlation model according to the calculated results, there
375 is a delayed response between the rainfall and landslide deformation in the study area, and there is a 5-
376 day lag time under a 56-day cycle. In summary, this area can be simulated by a rainfall-landslide
377 deformation hysteresis correlation model.

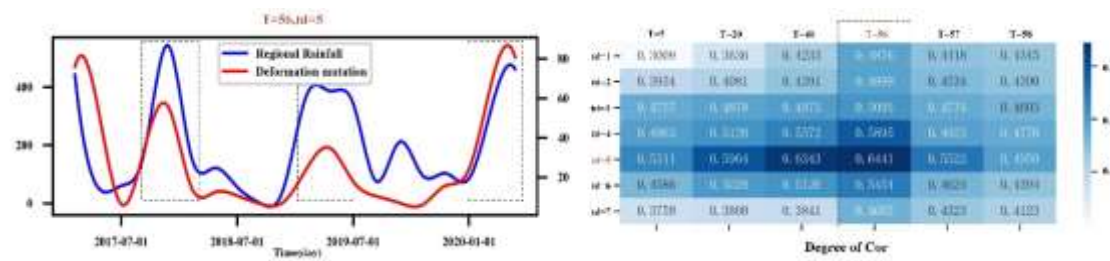


378
379
380

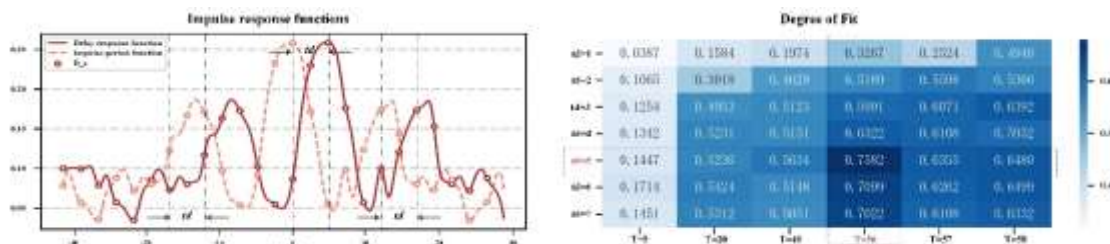
Figure. 5 Map of monitoring data at landslide site GDA10068. Used to calculate rainfall-triggered deformation value, mutation signals and the corresponding Kalman filter results



382 **Figure. 6(a)** This figure illustrates the process of monitoring signals for period clustering using the time domain correlation
 383 measure described and the signal time shifting. The correlation measure Cor is also measured quantitatively
 384



385 **Figure. 6(b)** This figure shows the quantitative calculation of the signal after the clustering and time-shifting operations. The
 386 value of Cor tells us the optimal T and td



387 **Figure. 6(c)** Response function construction and quantitative calculation results for correlated signals. The value of Fit tells us
 388 the optimal T and td
 389

390
391
392

Figure. 6 Map of the results of the test using the time-domain correlation quantitative analysis model at landslide site GDA10068

Table. 4 Table of quantitative analysis results of monitoring points in the landslide area

Landslide area	Monitoring sites	T	td	Cor_T	Cor_{td}	Fit_T	Fit_{td}	M
TMS landslide	1220	48	0	0.6775	0.1162	0.7521	0.2236	
	1235	48	0	0.7217	0.2158	0.7956	0.2665	Rainfall-landslide
	1243	50	0	0.6022	0.3547	0.7142	0.2737	deformation
OT landslide	MJ01	58	0	0.6931	0.2422	0.8015	0.2483	consistency model
	MJ14	58	0	0.7839	0.2216	0.8657	0.1157	M_1
	FA35	58	0	0.6236	0.3188	0.6934	0.2685	
XP landslide	GDA10068	56	5	0.2574	0.6441	0.2748	0.7582	
	GDA10077	56	5	0.2031	0.7105	0.1778	0.7938	Rainfall-landslide
	GDA10357	56	5	0.1852	0.7190	0.1862	0.8114	deformation
XSP landslide	FJ02	49	18	0.2276	0.7227	0.1421	0.8624	hysteresis model
	FJ03	50	21	0.2185	0.7195	0.1488	0.8473	M_2
	FJ04	52	20	0.2939	0.6168	0.3162	0.7025	
HJWC landslide	FJ02	23	0	0.1913	0.1898	0.2483	0.2737	Rainfall landslide
	FJ05	12	6	0.3395	0.3188	0.2926	0.1974	deformation
	FJ09	10	10	0.0674	0.2483	0.1737	0.2454	turbulence model M_3

393

Discussion

394

Table 4 shows all the proposed index parameters summarized by all the monitoring points through the above calculation process, which can meet the judgment requirements of the time-domain correlation model constructed in this article.

397

(1) According to the calculation results for the TMS landslide and the OT landslide model, there is a periodic correlation between the rainfall at the monitoring points and the landslide deformation, and the response function constructed by the above signals is expressed as a pulse period function $\varphi(T)$; at the same time period T , the signal correlation and function fitting degree under clustering are both greater than the correlation degree and fitting degree of the time shift td involved in the calculation and correspond to the consistent correlation model; therefore, such areas can be separately measured to determine the historical landslide deformation and displacement based on the amount of rainfall. Periodic accumulations of 48-50 days and 58 days can be used to predict consistent changes in future landslide motion.

406

(2) According to the model calculation results for the XP landslide and the XSP landslide, there is a periodic correlation between the rainfall at the monitoring points and the landslide deformation, and there is a certain signal time shift, and the response function shows a delayed response function $\varphi(td)$. The signal correlation degree and function degree involved in the calculation of the time shift td are greater than the correlation degree and the degree of fit under the clustering at period T , which corresponds to the hysteresis correlation model; therefore, there is a certain lag between the rainfall and landslide deformation in the above areas. Periodic changes in duration need to be analyzed in advance by a time shift when predicting future changes to obtain more adequate warning times.

414

(3) The model calculation results between the rainfall and landslide deformation at the HJWC landslide monitoring point all correspond to the turbulent correlation model. Therefore, it is not possible to provide a preliminary warning of landslide deformation based on rainfall alone in this area; rather, the additional analysis of other monitoring information is required.

415

416

417

418 Rainfall data are easy to obtain and constitute relatively stable monitoring data, and only surface
419 deformation data are needed to study the significant changes in landslide disasters to achieve effective
420 early warnings(Yue-li et al. 2016, Ze-lin et al. 2020). The method proposed in this paper involves a
421 calculation model for the signal correlation in the time domain. The proposed model can not only
422 quantitatively describe the motion of landslide deformation affected by rainfall but also determine
423 different correlation models based on the rainfall and landslide deformation and calculate the differences
424 between the two under different models. Compared with the existing methods, this time-domain
425 correlation feature also possesses a certain degree of universality and scalability when there is no ultra-
426 long time sequence and high-precision monitoring data. In particular, the time-domain correlation model
427 proposed herein is universal and can be used as a general judgment index for all rainfall-triggered
428 landslide disasters; moreover, the complexity of the response calculation method is low. Hence, this
429 model is suitable for supporting the parallel computing of short-term data from multiple monitoring
430 points on large-scale landslides, which is useful for periodic monitoring.

431 However, for landslide areas with turbulent patterns, it is difficult to obtain regular correlation
432 changes between the regional rainfall and landslide deformation(Zhiyun et al. 2020). Occasionally, large
433 fluctuations in cycles and time shifts occur in the same area. Therefore, further research can focus on
434 strengthening the correlation analysis of monitoring data with a relationship between the reservoir water
435 level and landslide deformation to improve the model indicators of rainfall-triggered landslides and other
436 types of landslides and more accurately establish multifactor constrained time-domain correlation models.
437 Nevertheless, this study provides a scientific and accurate basis for faster and more accurate landslide
438 warnings.

439 **Conclusions**

440 This paper proposes a method for the quantitative analysis of regional rainfall-landslide deformation
441 responses based on a time-domain correlation model. Considering the problem that the existing methods
442 have difficulty achieving short-term abnormal landslide deformation predictions through environmental
443 rainfall factors, the proposed model is established by using probability statistics and signal processing.
444 Rainfall factors are extracted and analyzed from multimodal landslide monitoring data, and a universal
445 correlation model for different landslide areas is constructed by mining potential and deep correlations
446 between temporal and spatial features. Furthermore, through a quantitative correlation measure, the
447 consistent correlation period and the hysteresis time shift caused by regional rainfall affecting landslide
448 deformation can be obtained, and finally, an effective prediction of landslide deformation can be achieved.
449 Experiments were conducted on rainfall and landslide deformation monitoring data at five landslide
450 locations in Fengjie County, Chongqing(Shen 2011, Yang et al. 2012). The results showed that the
451 rainfall-landslide deformation of the XP landslide and XSP landslide in hidden hazard areas exhibits a
452 delayed correlation. In contrast, the correlation model for the hidden hazard areas of the TMS landslide
453 and OT landslide shows a consistent correlation, verifying the feasibility of this method in studying the
454 deformation of rainfall-triggered landslides. For areas with disorderly correlations, due to the complex
455 causes of landslides, the external hazards affecting their deformation are not equally important, and for
456 some areas, it is difficult to analyze such deep correlations using only rainfall monitoring data. Therefore,
457 different influencing factors such as reservoir water levels should be added.

459 **Reference**

460 ADEL A, ST PHANE L, FRAN OIS N AND BRUNO C Recent Advances in Modeling Landslides
461 and Debris Flows. Springer International Publishing, 2015 p.

462 ADINEH F, MOTAMEDVAZIRI B, AHMADI H AND MOEINI A. 2018. Landslide susceptibility
463 mapping using Genetic Algorithm for the Rule Set Production(GARP) model.
464 Journal of Mountain Science 15: 2013-2026.

465 Egu General Assembly Conference, 2016. p.

466 CHUAN YE, KUN S AND GANG LH. 2010. Applicability of Time Domain Reflectometry for
467 Yuhuangge Landslide Monitoring. Journal of Earth Science 21: 856-860.

468 DE-YING L, YI-QING S, KUN-LONG Y, FA-SHENG M, GLADE T AND LEO C. 2019. Displacement
469 characteristics and prediction of Baishuihe landslide in the Three Gorges
470 Reservoir. Journal of Mountain Science 16: 2203-2214.

471 DONG J, LU ZG, SUN ZH, PENG ZT, XIA YW, SU JQ, FENG J, YUAN HY, HUA L AND TANG J.
472 2012. Transforming characteristic of phase-shift from frequency-domain to
473 time-domain in frequency-domain holography. Optics & Laser Technology 44:
474 594-599.

475 DU Y, HUANG G, ZHANG Q, GAO Y AND GAO Y. 2020. Asynchronous RTK Method for Detecting
476 the Stability of the Reference Station in GNSS Deformation Monitoring. Sensors
477 20.

478 FERRO V, CAROLLO FG AND SERIO MA. 2020. Establishing a threshold for rainfall induced
479 landslides by a kinetic Energy Duration relationship. Hydrological Processes.

480 GANG GF. Analysis of landslide development patterns and hazards in the Wenchuan
481 earthquake. Masters, Chengdu University of Technology.

482 GUANGMING LI, SHIGUANG XU, WANG Y AND SHUIYUN TU. 2016. Research on the instability
483 mechanism and treatment measures of the filled soil Landslide under heavy
484 rainfall. Journal of China Institute of Water Resources & Hydropower Research.

485 HUAN C. 2016. Analysis of Numerical Simulation of Wading Landslide in Three Gorges
486 Reservoir Area Based on Outang Landslide. Mathematical Modelling of
487 Engineering Problems 3.

488 HUNTER IW, KEARNEY RE AND JONES LA. 1987. Estimation of the conduction velocity of
489 muscle action potentials using phase and impulse response function techniques.
490 Medical & Biological Engineering & Computing 25: 121-126.

491 LI L, YAO X, YAO J, ZHOU Z AND LIU X. 2019. Analysis of deformation characteristics
492 for a reservoir landslide before and after impoundment by multiple D-InSAR
493 observations at Jinshajiang River, China. Natural Hazards 98.

494 LI X AND ZHAO J. 2019. An overview of particle-based numerical manifold method and
495 its application to dynamic rock fracturing. Journal of Rock Mechanics and
496 Geotechnical Engineering 11: 684-700.

497 MBACHU CB. 2020. Height Adjustable Sine (HAS) Window Function for Impulse Response
498 Modification of Signal Processing Systems. European Journal of Engineering
499 Research & Science 5: 367-374.

500 MUCCHI L, MOROSI S, DEL RE E AND FANTACCI R. 2004. A new algorithm for blind adaptive
501 multiuser detection in frequency selective multipath fading channel. IEEE
502 Transactions on Wireless Communications 3: 235-247.

503 QIU-XIANG H, XIANG-TAO X, P.H.S.W.KULATILAKE AND FENG L. 2020. Formation mechanism
504 of a rainfall triggered complex landslide in southwest China. Journal of
505 Mountain Science 17: 1128-1148.

506 1989. p.

507 SHEN LS. 2011. Study on the development pattern and instability mechanism of cascading
508 landslides on the reservoir bank in the Three Gorges reservoir area. Masters,
509 Northwest Agriculture and Forestry University.

510 SHU-LIN R, ZHI-GANG T, MAN-CHAO H, SHI-HUI P, MENG-NAN L AND HAO-TIAN X. 2020.
511 Stability analysis of open-pit gold mine slopes and optimization of mining
512 scheme in Inner Mongolia, China. *Journal of Mountain Science* 17: 2997-3011.

513 SKI JM AND OWCZAREK AJ. 2005. A time-domain-constrained fuzzy clustering method and
514 its application to signal analysis. *Fuzzy Sets & Systems* 155: 165-190.

515 TAO W, JIA-MEI L, JU-SONG S, MENG-TAN G AND SHU-REN W. 2020. Probabilistic seismic
516 landslide hazard assessment: a case study in Tianshui, Northwest China.
517 *Journal of Mountain Science* 17: 173-190.

518 TIPING D, JIANFEI G, SHIHONG T, GUOYU S, FENG C, CHENGYU W, XURONG L AND DAN H. 2014.
519 Chemical and Isotopic Characteristics of the Water and Suspended Particulate
520 Materials in the Yangtze River and Their Geological and Environmental
521 Implications. *Acta Geologica Sinica (English Edition)* 88: 276-360.

522 TOSHIAKI, SAMMORI, YOICHI, OHKURA, HIROTAKA, OCHIAI, HIKARU AND KITAHARA. Effects of
523 Soil Depth on Rain-induced Landslide. *Journal of the Japan Society of Erosion
524 Control Engineering* 48.

525 VALLET A, CHARLIER JB, FABBRI O, BERTRAND C, CARRY N AND MUDRY J. 2016. Functioning
526 and precipitation-displacement modelling of rainfall-induced deep-seated
527 landslides subject to creep deformation. *Landslides* 13: 653-670.

528 VAN DH, T. 2014. Experimental dynamic substructuring using direct time-domain
529 deconvolved impulse response functions.

530 WANG J, XIAO L, ZHANG J AND ZHU Y. 2020. Deformation characteristics and failure
531 mechanisms of a rainfall-induced complex landslide in Wanzhou County, Three
532 Gorges Reservoir, China. *Landslides* 17: 419-431.

533 WANG Y, YUE J, DONG Y AND HU Z. 2016. Review on Kernel based Target Tracking for
534 Autonomous Driving. *Journal of Information Processing* 24: 49-63.

535 XIN M. 2016. Landslide risk assessment techniques considering the activity state of
536 slopes. Masters, Chengdu University of Technology.

537 YAN Y, DA-SHEN Y, DONG-XIAN G, SHENG H, ZI-ANG W, WANG H AND SHU-YAO Y. 2019. Disaster
538 reduction stick equipment: A method for monitoring and early warning of
539 pipeline-landslide hazards. *Journal of Mountain Science* 16: 2687-2700.

540 YANG L, LU RN, TAN DJ, XIE HB AND LUO ZF. 2012. Study on Interpretation of Landslides
541 Based on Gis — Taking New Fengjie County in Chongqing as an Example. *Applied
542 Mechanics and Materials* 1975.

543 YI-TING W, CHRISTOFFEL SA, WILLEM B AND QING-TAO C. 2015. Using Statistical Learning
544 Algorithms in Regional Landslide Susceptibility Zonation with Limited
545 Landslide Field Data. *Journal of Mountain Science* 12: 268-288.

546 YIN Y, HUANG B, WANG W, WEI Y, MA X, MA F AND ZHAO C. 2016. Reservoir-induced
547 landslides and risk control in Three Gorges Project on Yangtze River, China.
548 *Journal of Rock Mechanics and Geotechnical Engineering* 8: 577-595.

549 YUAN L. 2005. Research on forecast and early warning methods of regional rainfall-

550 type landslides. PhD, China University of Geosciences (Beijing).
551 YUE-LI C, DE-HUI C, ZE-CHUN L AND JUN-BAO H. 2016. Preliminary studies on the dynamic
552 prediction method of rainfall-triggered landslide. Journal of Mountain
553 Science 13: 1735-1745.
554 ZE-LIN Z, TAO W AND SHU-REN W. 2020. Distribution and features of landslides in the
555 Tianshui Basin, Northwest China. Journal of Mountain Science 17: 686-708.
556 ZHIYUN D, XINRONG L, YONGQUAN L, SHULIN L, YAFENG H, JINHUI L AND YILIANG T. 2020.
557 Model test and numerical simulation on the dynamic stability of the bedding
558 rock slope under frequent microseisms. Earthquake Engineering and Engineering
559 Vibration 19: 919-935.
560 ZHU QING MS, DING YULIN, QI HUA, HE XIAOBO, CAO ZHENYU. 2017. Knowledge-guided Gross
561 Errors Detection and Elimination Approach of Landslide Monitoring Data.
562 Geomatics and Information Science of Wuhan University: 42(44).
563

Figures

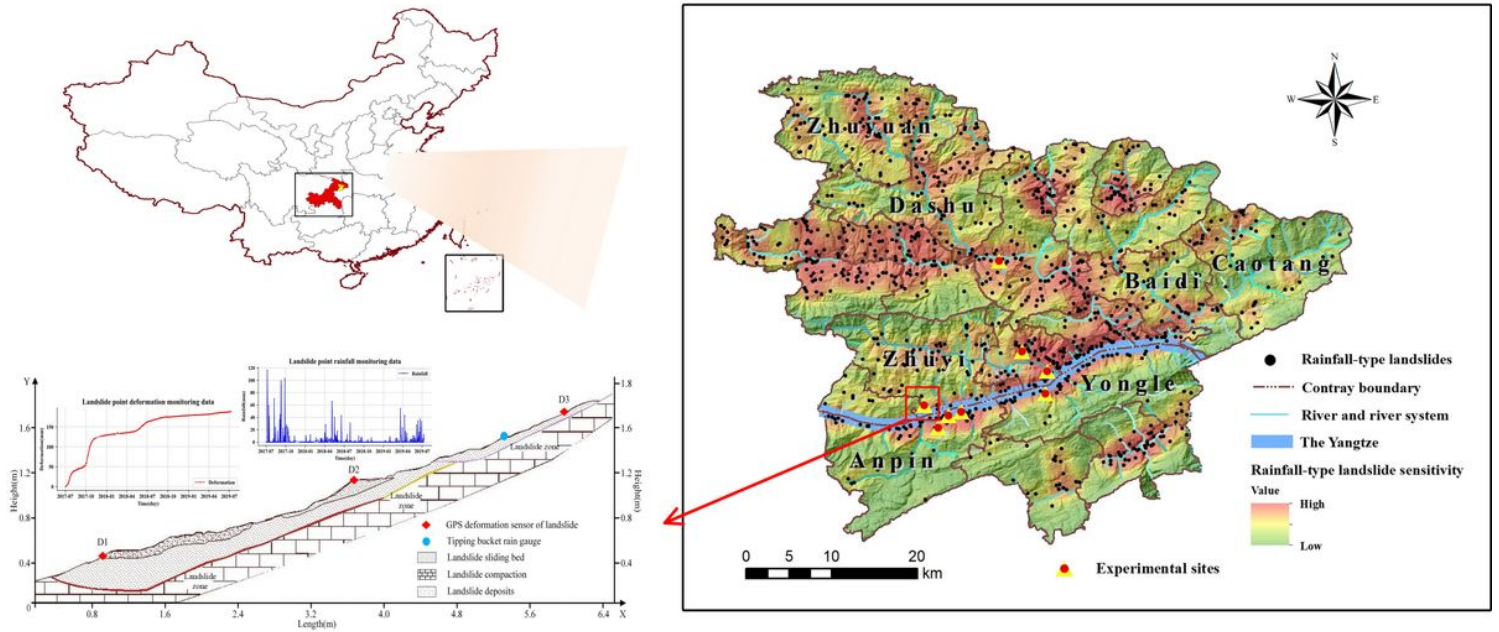


Figure 1

The tests were conducted at rainfall-triggered landslides such as the Xinpu landslide in Fengjie County, Chongqing, China. Note: The designations employed and the presentation of the material on this map do not imply the expression of any opinion whatsoever on the part of Research Square concerning the legal status of any country, territory, city or area or of its authorities, or concerning the delimitation of its frontiers or boundaries. This map has been provided by the authors.

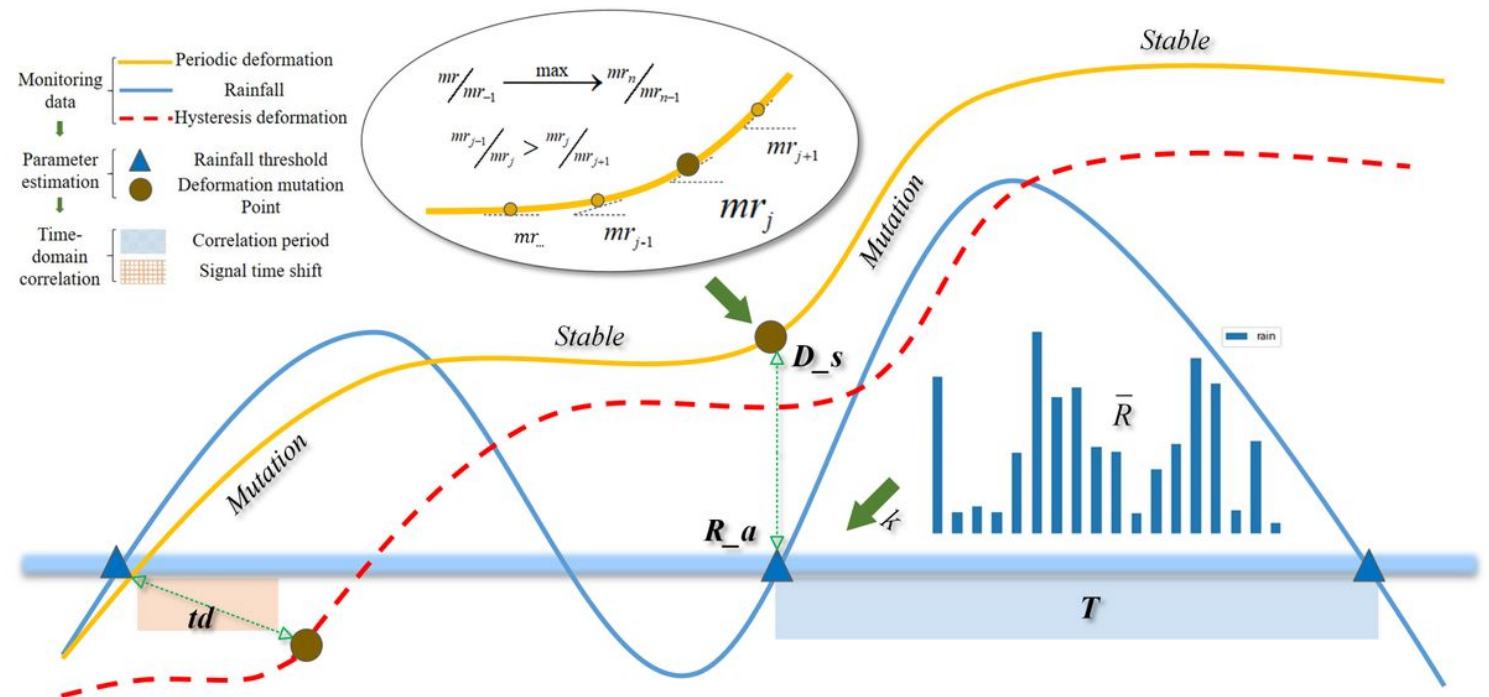


Figure 2

Conceptual diagram of regional rainfall-landslide deformation time-domain correlation measurement

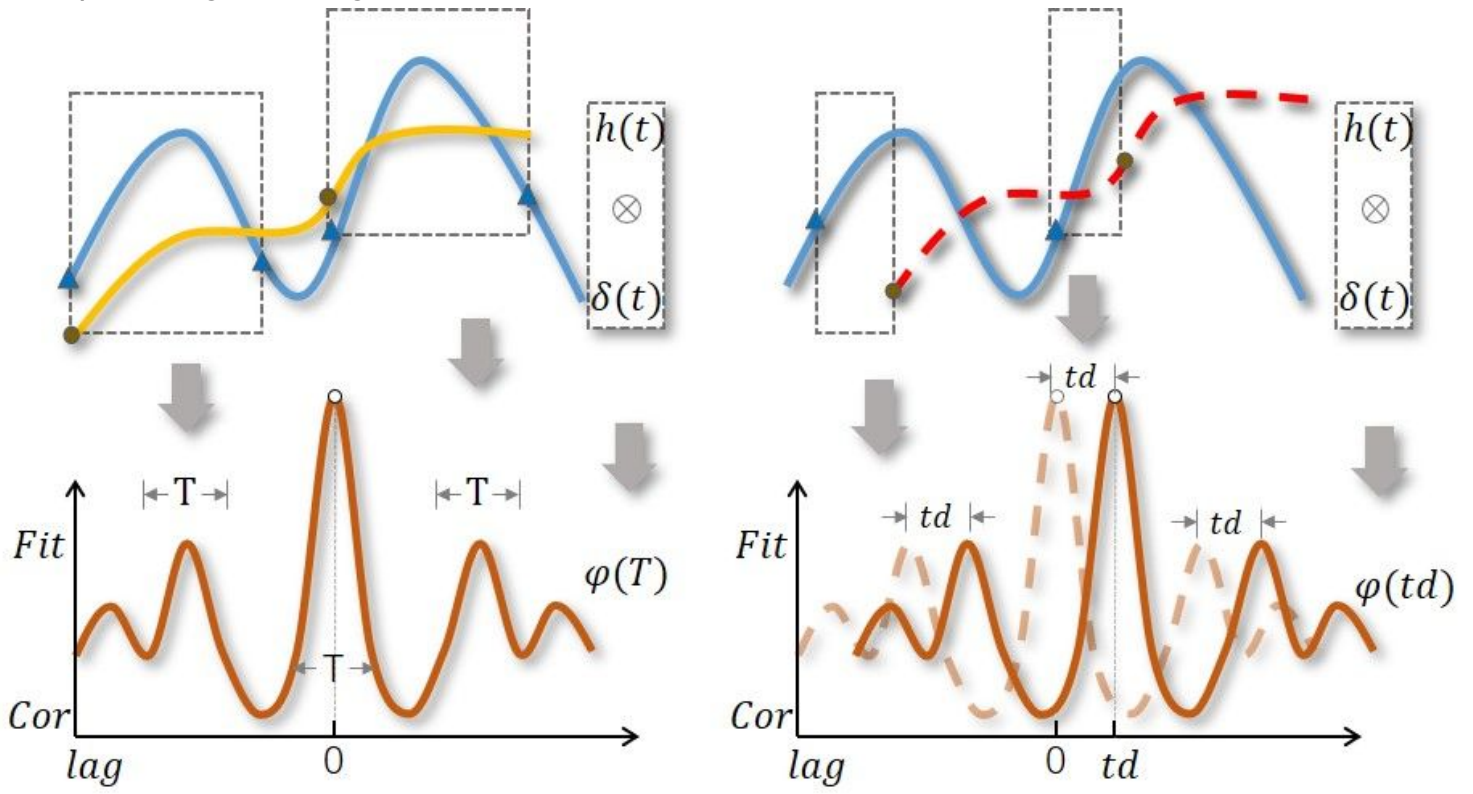


Figure 3

Schematic diagram for calculating time-domain correlation measures based on impulse response functions

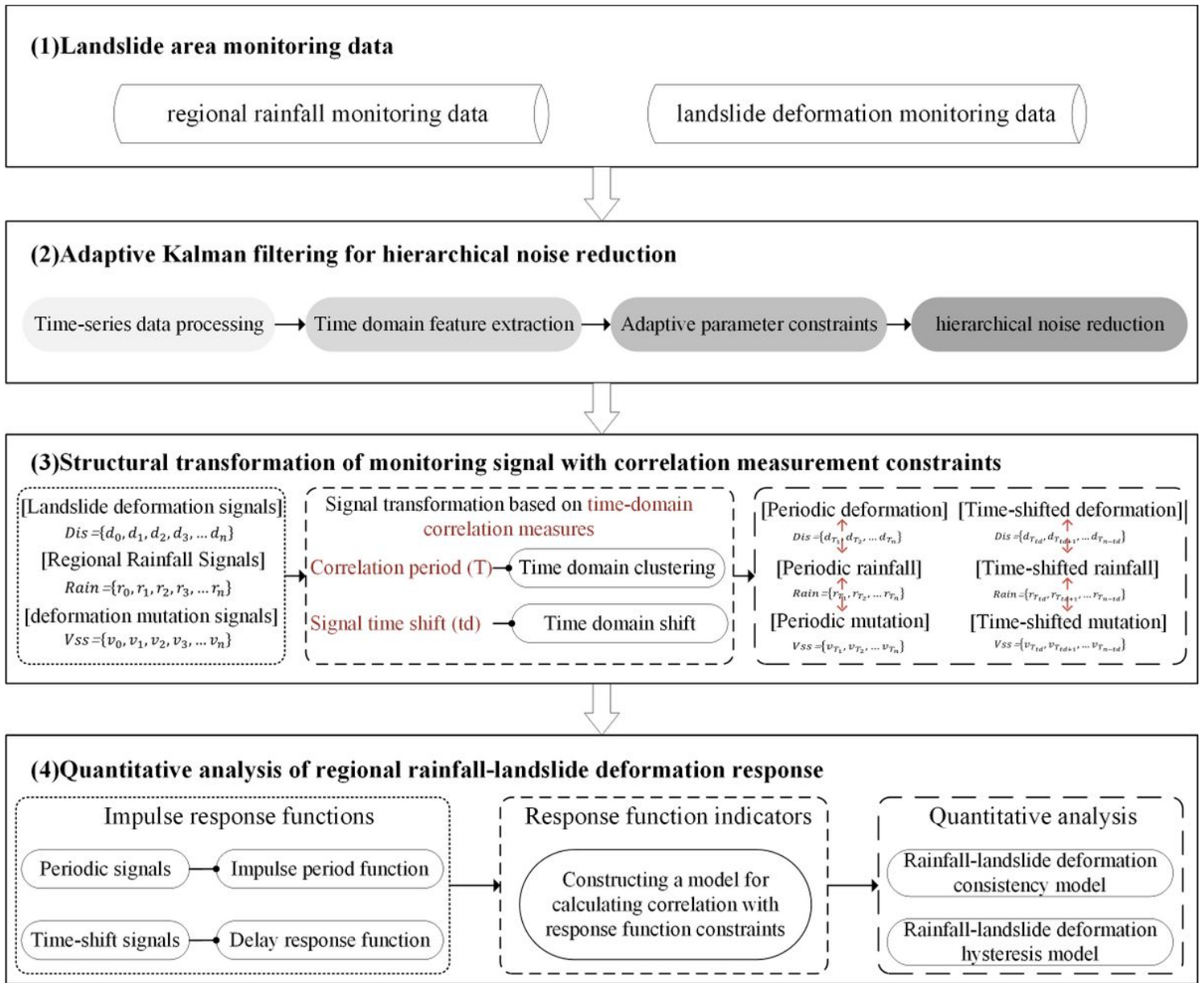


Figure 4

Flow chart of the regional rainfall-landslide deformation quantitative response analysis algorithm

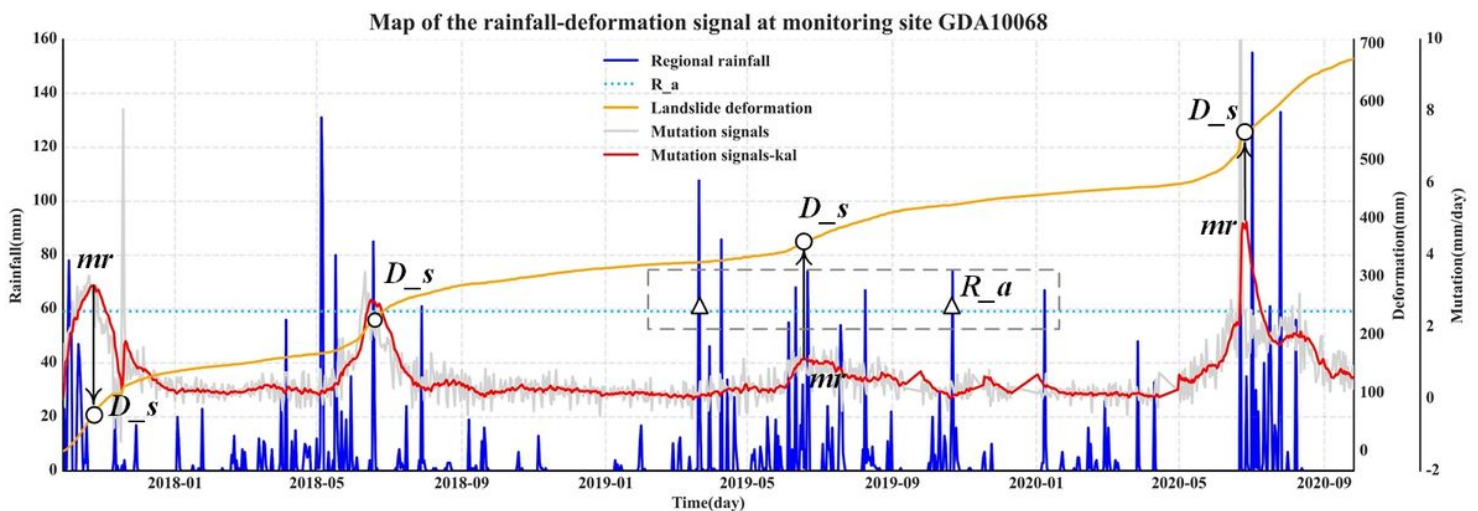


Figure 5

Map of monitoring data at landslide site GDA10068. Used to calculate rainfall-triggered deformation value, mutation signals and the corresponding Kalman filter results

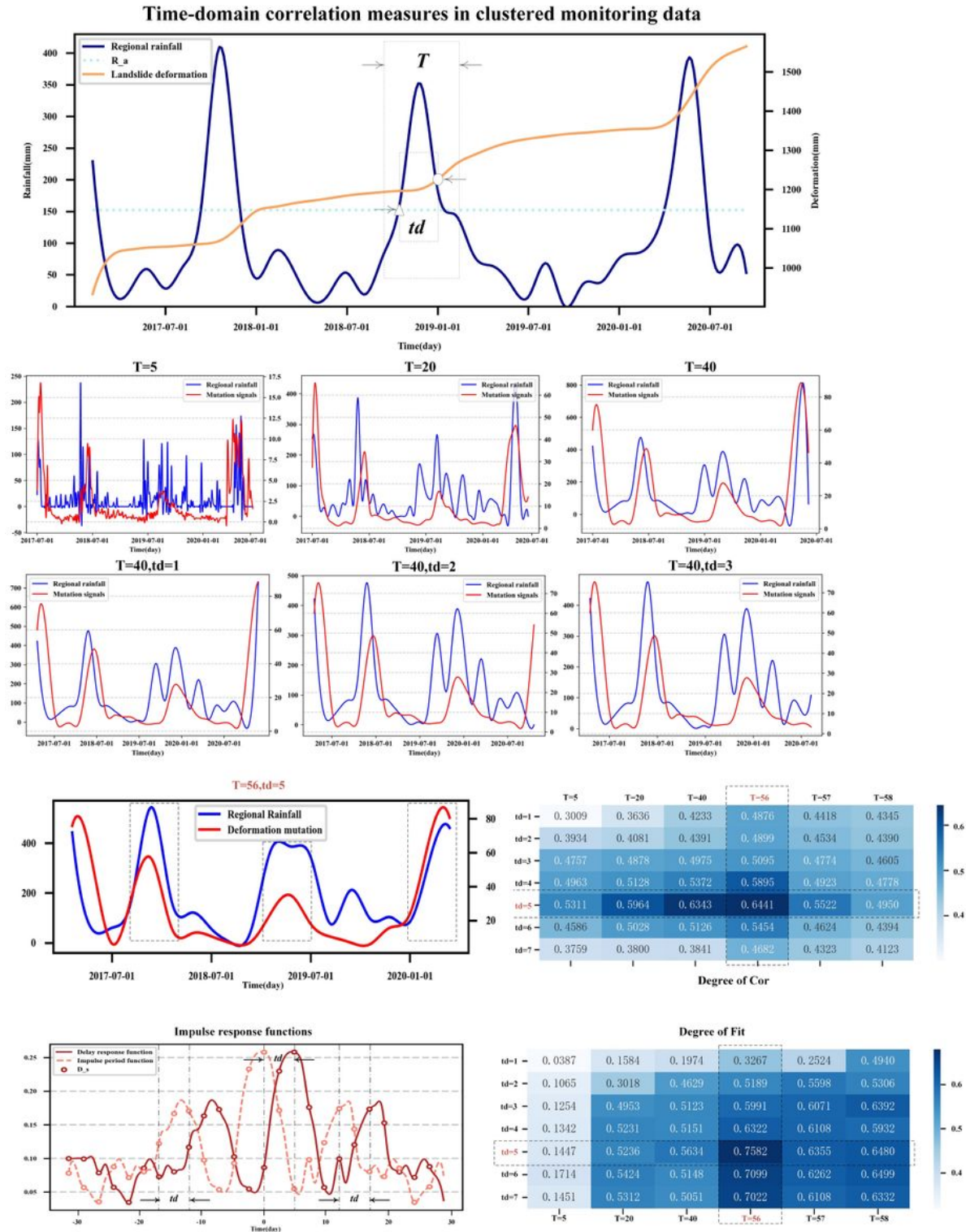


Figure 6

Map of the results of the test using the time-domain correlation quantitative analysis model at landslide site GDA10068 (a) This figure illustrates the process of monitoring signals for period clustering using the time domain correlation measure described and the signal time shifting. The correlation measure Cor is also measured quantitatively (b) This figure shows the quantitative calculation of the signal after the clustering and time-shifting operations. The value of Cor tells us the optimal T and td (c) Response function construction and quantitative calculation results for correlated signals. The value of Fit tells us the optimal T and td